INTERNATIONAL ATOMIC ENERGY AGENCY

19th IAEA Fusion Energy Conference
Lyon, France, 14-19 October 2002

IAEA-CN-94/EX/D1-2

Exhaust, ELM and Halo physics using the MAST Tokamak

G.F. Counsell 1), J-W. Ahn 1), R.H. Cohen 2), A. Kirk 1), P. Helander 1), R. Martin 1), D.D Ryutov 2), A. Tabasso 1), H.R. Wilson 1), Y. Yang 3) and the MAST team

1) EURATOM/UKAEA Fusion Association, Culham Science Centre, OX14 3DB. UK.
2) Lawrence Livermore National Laboratory, Livermore, CA 94551
3) Institute of Plasma Physics, Hefei, 230031, P.R.China.

Email contact of main author: glenn.counsell@ukaea.org.uk

Exhaust, ELM and Halo physics using the MAST Tokamak

G.F. Counsell 1), J-W. Ahn 1), R.H. Cohen 2), A. Kirk 1), P. Helander 1), R. Martin 1), D.D. Ryutov 2), A. Tabasso 1), H.R. Wilson 1), Y. Yang 3) and the MAST team

1) EURATOM/UKAEA Fusion Association, Culham Science Centre, OX14 3DB. UK.
2) Lawrence Livermore National Laboratory, Livermore, CA 94551
3) Institute of Plasma Physics, Hefei, 230031, P.R.China.

Email contact of main author: glenn.counsell@ukaea.org.uk

Abstract. The scrape-off layer (SOL) and divertor target plasma of a large spherical tokamak (ST) is characterised in detail for the first time. Scalings for the SOL heat flux width in MAST are developed and compared to conventional tokamaks. Modelling reveals the significance of the mirror force to the ST SOL. Core energy losses, including during ELMs, in MAST arrive predominantly (>80%) to the outboard targets in all geometries. Convective transport dominates energy losses during ELMs and MHD analysis suggests ELMs in MAST are Type III even at auxiliary heating powers well above the L-H threshold. ELMs are associated with a poloidally and/or toroidally localised radial efflux at ~1 km/s well into the far SOL but not with any broadening of the target heat flux width. Toroidally asymmetric divertor biasing experiments have been conducted in an attempt to broaden the target heat flux width, with promising results. During vertical displacement events, the maximum product of the toroidal peaking factor and halo current fraction remains below 0.3, around half the ITER design limit. Evidence is presented that the resistance of the halo current path may have an impact on the distribution of halo current.

1. Introduction

The boundary and divertor plasma of a large spherical tokamak (ST) has been characterised in detail for the first time, using the extensive edge diagnostics now available on the MAST device. An overview of MAST parameters and operation is provided in [1]. Studies have been conducted to investigate the impact of the extreme ST geometry on power and particle fluxes to the plasma facing components, including during transient events such as ELMs, and to evaluate the nature of halo currents flowing in the divertor structures during vertical displacement events (VDEs).

MAST operates in a double-null configuration and is equipped with a simple, open divertor [2]. Typically the double-null is slightly asymmetric, with the two X-points lying on separate flux surfaces, the disconnected double-null configuration (DDN). The characteristics of the core plasma in L and H-mode are broadly similar to conventional devices of a similar size, such as Asdex-Upgrade or DIII-D, allowing the specific impact of ST geometry on the boundary plasma to be assessed. Aspects of that geometry, such as a large parallel gradient in the magnitude of the magnetic field along the SOL and a factor four difference between the surface area of the outer and inner separatrices, play a key role in determining, for example, divertor target power loads.

Section 2 introduces the parameters of the MAST scrape-off layer (SOL), explores the balance of heat flux between the four divertor targets, for a range of plasma geometries and discusses efforts both to computationally model the SOL and to develop empirical scalings for the SOL heat flux width. Section 3 characterises the ELMs observed in MAST H-modes and discusses their impact on the pedestal, SOL and target plasmas. Section 4 introduces novel experiments to broaden the target heat flux width by toroidally asymmetric biasing of the divertor targets. Section 5 explores the currents observed to flow in the centre column, divertor and internal poloidal field coils during VDEs. Lastly, section 6 provides some concluding remarks.

2. The MAST Scrape-off layer

2.1 SOL parameters

The SOL in MAST has been characterised for both L-mode and ELMy H-mode phases of typical DDN plasmas at plasma currents, I_p up to 1 MA and with up to 2.5 MW of neutral beam heating, P_{NBI}. For line-averaged core plasma densities, $\bar{n}_e < 2\text{x}10^{19}\,\text{m}^{-3}$, the outboard SOL in L-mode remains in the sheath-limited regime. The strike-point electron temperatures are, $T_t \sim 25 - 40$ eV and the densities are, $n_t \sim 0.5 - 1\text{x}10^{18}\,\text{m}^{-3}$ in this regime, where n_t rises approximately linearly with $\bar{n}_e$ and the collisionality in the SOL, ν^* is typically of order unity ($\nu^* \equiv L_{//}/\lambda_{ee}$, where $L_{//}$ is the parallel connection length in the SOL and λ_{ee} is the e-e collisional mean free path). For higher densities, $2\text{x}10^{19}\,\text{m}^{-3} < \bar{n}_e < 3.5\text{x}10^{19}\,\text{m}^{-3}$, n_t rises at least parabolically with $\bar{n}_e$, T_t falls to 10 - 15 eV and ν^* rises to greater than 10, indicating a transition to the conduction-limited regime. At still higher densities, the ion saturation current, j_{sat} to Langmuir probes embedded in the targets begins to fall gradually, at least for plasmas with P_{NBI} up to 0.75 MW. This fall occurs at slightly lower densities for the inboard SOL than for the outboard, $\bar{n}_e \sim 3.0\text{x}10^{19}\,\text{m}^{-3}$, and at P_{NBI} up to at least 1MW (figure 1). In addition, the inboard SOL remains in the conduction-limited regime even for the lowest $\bar{n}_e$ explored.

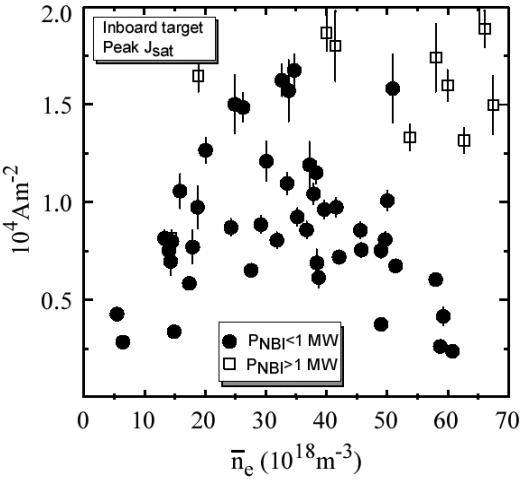

Figure 1: Peak j_{sat} at inboard target as a function of $\bar{n}_e$, in L-mode

The fall in j_{sat} with increasing $\bar{n}_e$ in L-mode discharges is accompanied by an increase in the ratio of D_γ to D_α emission from the targets and a gradual fall in T_t to less than 5 eV, as measured by the target probes [3]. These characteristics are consistent with radiative detachment at the targets and would correspond to a degree of detachment [4] of 6 for the outboard targets and 20 for the inboard at $\bar{n}_e \sim 6\text{x}10^{19}\,\text{m}^{-3}$ (from an extrapolated fit to the conduction limited regime in each case, assuming a parabolic dependence of j_{sat} on $\bar{n}_e$). At the roll-over, however, n_t is typically $2 - 3\text{x}10^{18}\,\text{m}^{-3}$, substantially lower than has been reported for detachment in other tokamaks. The mean free path for ionisation of recycled neutrals at such low densities is $\lambda_{ion} \sim 50$cm (*cf* $\lambda_{ion} < 1$cm in a typical JET discharge). λ_{ion} thus far exceeds scale lengths for the target region in MAST and would appear to be in contradiction to the conventional explanation for detachment, which relies on a strong feedback between recycling at the target and local re-ionisation. Further work is thus required to develop a quantitative understanding of the physical mechanisms underlying the apparent detachment in MAST. These mechanisms might include effects related to the large $\nabla_{//}B/B$ in the MAST SOL (see section 2.3) and the impact of leading edges on the toroidally separated divertor ribs [5].

As with conventional devices, characterisation of the MAST SOL in H-mode is difficult because of the impact of ELMs. ELM-averaged data for the outboard SOL is too scattered to make any firm conclusions but the inboard SOL would appear to remain in the conduction-limited regime even up to the highest $\bar{n}_e$ explored. What is clear is that there is no roll-over in ELM-averaged j_{sat}

with increasing $\bar{n}_e$ at either the outboard or inboard targets in H-mode. In order to investigate the MAST H-mode SOL in more detail and especially to investigate characteristics of the target plasma, fast Langmuir probe electronics combined with data box-car techniques were used to separately resolve the inter-ELM and ELM periods. The results are presented in sections 2.4/3.1.

2.2 SOL scalings

Data collected from MAST L-mode plasmas have been used to develop scalings for the mid-plane heat flux SOL width, Δ_h in terms of the major engineering parameters such as power flow across the separatrix, P_{SOL} and safety factor at the 95% flux surface, q_{95}. Δ_h will play a key role in determining divertor power loadings in next-step devices, such as ITER. Scalings developed for the ST significantly extend the parameter range explored in conventional devices, for example in toroidal field, and are in any case necessary for estimating the expected divertor power loadings in designs for future ST power plants. In the conduction-limited regime, a scaling of the form $\Delta_h \propto P_{SOL}^{-0.07\pm0.03}\bar{n}_e^{1.26\pm0.26}q_{95}^{0.84\pm0.23}$ provides a reasonable fit to data selected from L-mode discharges with an absence of strong MHD and for which the SOL was well fitted by an offset exponential (figure 2). In order to minimise the effects of co-linearity, dedicated campaigns were undertaken to explore the widest possible range of each parameter, whilst keeping the remainder as fixed as possible. The scaling seems to confirm the weak negative dependence of Δ_h on P_{SOL} noted for conventional devices and in scalings developed from multi-machine databases such as [6], which also shows a similar, though somewhat less strong, positive dependence with $\bar{n}_e$ and q_{95}. In symmetric double-null (CDN) discharges, separate analysis of data from the inner and outer SOLs yields similar scalings with P_{SOL}, $\bar{n}_e$ and q_{95} and, in addition, allows the scaling with local toroidal field, B_T to be evaluated over a wide range. B_T changes by a factor ~6 between the inner and outer SOL in MAST, whereas the field on axis, B_0 is typically varied by less than 50%. Preliminary analysis suggests a reasonably strong negative dependence, $\Delta_h \propto B_T^{-0.8}$. In addition to development of empirical SOL scalings, a range of dimensionally correct scalings for the SOL width, based on theoretical models for the cross-field heat diffusion coefficient, $\chi_\perp$ coupled with a classical parallel transport model [7] have been tested. A scaling derived from a resistive MHD interchange model for $\chi_\perp$ provides a best fit to the data and has the form $\Delta_h \propto P_{SOL}^{-2/5}\bar{n}_e^{14/15}q_{95}^{16/15}B_T^{-14/15}$, with similar dependencies to the empirical model except for the P_{SOL} index, which is rather more negative.

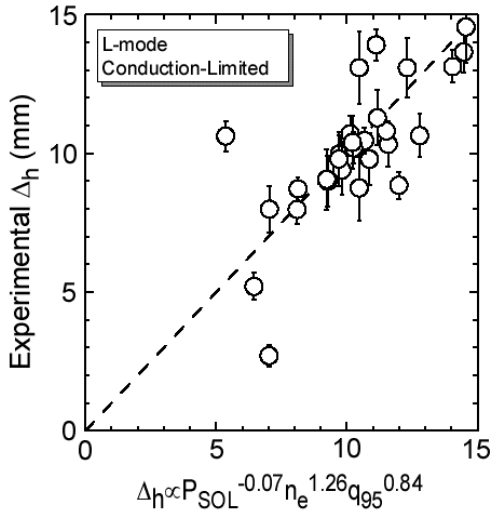

Figure 2: SOL scaling for outboard SOL in L-mode conduction limited regime

2.3 Modelling the SOL

In order to develop a more quantitative understanding of the MAST SOL, modelling has been undertaken using an OSM-EIRENE package [8] and a detailed comparison has been made with

results from a conventional tokamak, JET [9]. One key issue uncovered by this modelling is the significance of the mirror force for the ST SOL. This force is proportional to $\nabla_{//}B/B$, which is typically a factor 10 larger in an ST due to the low aspect ratio (figure 3) and can lead to large trapped particle fractions in the SOL (in low collisionality regimes). Changes in the charged particle velocity distributions near regions with large $|\nabla_{//}B/B|$ leads to the $\nabla_{//}B/B$ term representing an effective, upstream particle and momentum source, which can exceed sources at the targets (e.g. from ionisation and charge exchange) that are normally dominant in conventional tokamaks. The modelling indicates that the $\nabla_{//}B/B$ term could be responsible for driving strong flows in the upstream SOL of MAST, at a significant fraction of the Mach number, M. Preliminary measurements with a Mach probe mounted on a reciprocating probe at the outboard mid-plane in MAST appear to confirm the existence of upstream flows with M~0.2, comparable with the results from OSM. The specific impact of this term has been overlooked in modelling of conventional Tokamaks and the mirror term is in fact absent in some fluid models for the SOL. Although the mirror term is significantly smaller in conventional tokamaks, modelling of the JET SOL has shown that it may not be ignorable.

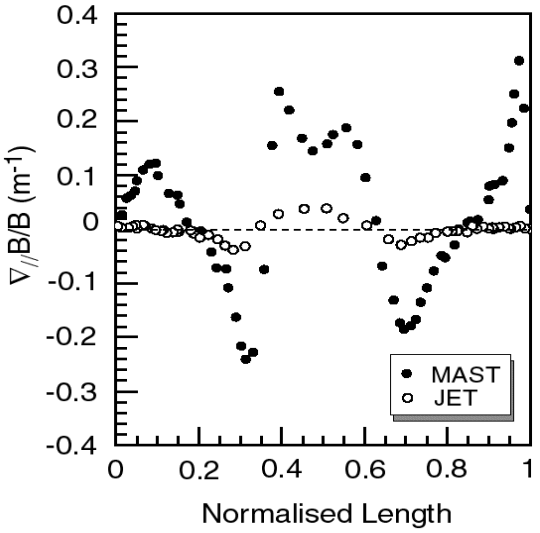

Figure 3: Variation of $\nabla_{//}B/B$ along the SOL from the outboard to inboard targets for typical MAST and JET discharges

2.4 Power accounting and balance

In L-mode, the total power observed to arrive at all four targets, using Langmuir probes, accounts for nearly 100% of P_{SOL} and is distributed mostly towards the outboard targets. The ratio of power arriving at the outboard to inboard targets is typically R_{oi}~30 for CDN configurations and is rather evenly distributed between the upper and lower targets. In fact, an exact up-down power balance is achieved for slightly asymmetric upper DDN configurations, as a result of the ion ∇B drift towards the lower X-point. In very asymmetric DDN configurations, approaching single-null, R_{oi} falls to ~4, roughly equal to the ratio of the outboard to inboard plasma surface area in MAST.

In ELMy H-mode, at most ~70% of P_{SOL} is accounted for by Langmuir probes at the target. There is no evidence for either increased radiation from the SOL or significant power deposition outside of the target region. The most probable explanation for this discrepancy is an increase in the ion to electron temperature ratio, T_i/T_e. The Langmuir probe analysis has power to the probes, $P = \gamma j_{sat} T_e$, where $T_i/T_e = 1$ is assumed in the sheath transmission coefficient, γ. If T_i/T_e is actually 3 or 4 in the H-mode SOL, γ and thus P will be underestimated by at least 30%. Further evidence for high ion temperatures in the SOL is provided from estimates of the parallel transit time during ELMs using D_α measurements and from charge exchange measurements of T_i at the pedestal.

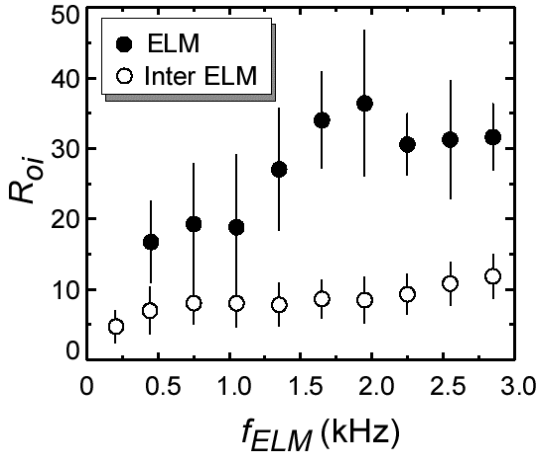

Figure 4: Power distribution between the outboard and inboard targets at ELM peaks and in inter-ELM periods with f_{ELM}

During inter-ELM periods, R_{oi} is a function of the ELM frequency, f_{ELM} and falls from $R_{oi} \sim 12$ at $f_{ELM} = 3$ kHz to a minimum of $R_{oi} \sim 4$ for $f_{ELM} < \sim 100$ Hz, figure 4. At the ELM peaks, however, R_{oi} rises significantly, to $R_{oi} \sim 30$ - 40 at $f_{ELM} > \sim 1.5$ kHz and $R_{oi} \sim 15$ at $f_{ELM} \sim 400$ Hz. Data is not yet available at lower f_{ELM} due to the difficulty of using data box-car techniques for low frequency events, however, extrapolating from $f_{ELM} > 400$ Hz indicates a minimum of $R_{oi} \sim 10$ even for $f_{ELM} < 100$ Hz. Thus, in typical ELMy H-modes on MAST, more than 90% of energy released during an ELM and observed at the targets is to the outboard side.

The data are consistent with transport into the SOL being driven predominantly by poloidally symmetric processes in quiescent ELM-free periods, and thus being distributed roughly according to the 4:1 ratio of outboard to inboard separatrix surface areas. In L-mode and during ELMs, however, the transport may be augmented by poloidally asymmetric processes that are more prominent at the outboard side, such as turbulence related to the bad curvature and low field on the outboard mid-plane.

3. MAST ELMy H-mode operation

3.1 ELM characterisation

ELMy H-modes have been observed on MAST with pedestal densities in the range, $1\text{x}10^{19}$ m^{-3} < n_p < $5\text{x}10^{19}$ m^{-3} and with pedestal temperature, 60 eV < T_p < 190 eV. T_p has been plotted against edge density, n_p (both normalised to B_0/q_{95}) for a broad range of ELMy H-mode regimes from Ohmic plasmas up to $P_{NBI} \sim 2.5$ MW, figure 5. The normalisation allows the region of instability to n=∞ ideal ballooning modes to more self-consistently presented on the diagram. The boundary was derived by extrapolation from the equilibrium and pressure profile for shot 6252, which is just in the region of instability, using the IDBALL code [10].

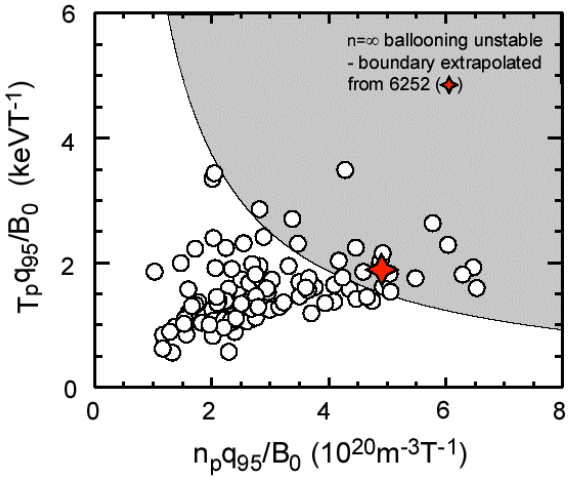

Figure 5: Normalised pedestal temperature and density for a broad range of ELMy H-modes

The bulk of ELMy H-mode discharges examined are stable to ballooning modes but in a region of instability to peeling modes (driven by the edge bootstrap current). These highly localised instabilities may be responsible for Type III ELMs. A significant number of discharges, however, are predicted to be unstable to n=∞ ideal ballooning modes and thus might be expected to exhibit Type I characteristics. More detailed analysis of shot 6252 using the ELITE code [11] though shows it to be stable up to n ~ 60 due to stabilising finite n correction terms, which are

enhanced in MAST by the narrowness of the pedestal [12]. Since Type I ELMs are normally associated with instability at much lower n (typically <7), there is thus no clear evidence from MHD analysis for Type I ELMs on MAST, even at the highest P_{NBI}. This conclusion is supported by analysis of the collisionality at the top of the pedestal, n^*_{ped} and the fractional energy loss during ELMs. The discharges presented in figure 5 have a mean n^*_{ped} ~ 2.1±1.3, the high collisionallity being a result of the steep edge density gradients normally observed in MAST H-modes. The fractional loss of energy from the core during ELMs, $\Delta W_{ELM}/W$ increases with falling f_{ELM} from ~1% at f_{ELM} ~ 1 kHz to a maximum of ~3.5% for discharges with the lowest frequencies regularly encountered, f_{ELM} ~ 35 Hz. The fraction of heating power P_{heat} ($\equiv P_{NBI}+P_{\Omega}$, the Ohmic heating power) transported by the ELMs, $\Delta W_{ELM} f_{ELM}/P_{heat}$ for these low f_{ELM} discharges is ~5% (ΔW_{ELM} is typically 2 – 3 kJ in these cases). These discharges correspond to those furthest beyond the n=∞ ideal ballooning mode boundary but both $\Delta W_{ELM}/W$ and $\Delta W_{ELM} f_{ELM}/P_{heat}$ are significantly lower than reported for Type I ELMs in conventional devices of a similar size. For example, Asdex-Upgrade reports $\Delta W_{ELM} f_{ELM}/P_{heat}$ ~ 30% for Type I ELMs [13]. The ELM losses on MAST are modest, even for the discharges with the highest auxiliary heating powers, and the edge MHD stability characteristics are not those expected of Type I ELMs. Nevertheless, the plasma confinement is at least as good as predicted by scaling laws, such as IPB98(y,2). The normalised confinement H_H ($\equiv t_E / t_E^{IPB98(y,2)}$, where t_E is the energy confinement time) rises with falling f_{ELM} and exceeds H_H of 1.2 for the lowest f_{ELM} discharges.

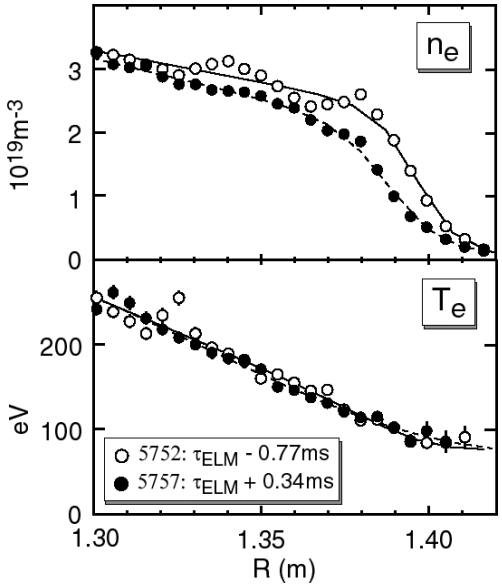

Figure 6:Edge density and temperature profiles before and just after an ELM

3.2 Impact on the target, SOL and pedestal

Peak heat flux densities, P_0 at the outboard targets rise by a factor ~3 during typical ELM events and, for f_{ELM} < ~2 kHz, this is accompanied by a shift in the strike-point location of several centimetres, although there is little change in the target heat flux width, Δ^t_h. As a result P_0 rises roughly linearly with P_{SOL} and for P_{SOL} ~ 2 MW, the highest value so far explored, P_0 reaches ~1.5 MWm^{-2} in inter-ELM periods and rises to ~4.0 MWm^{-2} at the ELM peaks. At the inboard targets P_0 rises to ~1.5 MWm^{-2} at the highest P_{SOL} and increases by less than 25% during ELMs, consistent with a high value of R_{oi} and the bulk of ELM energy flowing to the outboard targets.

Thomson scattering profiles of density and temperature across the pedestal region have been obtained from nominally identical ELMy H-mode discharges during an inter-ELM period, 770 μs before the time of peak divertor D_α emission, τ_{ELM} – 770 μs, and just after the ELM peak, in the foot of the decay in D_α emission, τ_{ELM} + 340 μs (figure 6). These indicate that ΔW_{ELM} in MAST is dominated by convective losses, with large falls in density across the pedestal region but little change to the edge temperature profile, i.e. $\langle T\rangle\Delta n >> \langle n\rangle\Delta T$. Analysis of the drop in $\bar{n}_e$ using an interferometer with 20 μs time resolution, indicates that convective losses can account for the observed ΔW_{ELM}, even for H-modes with P_{NBI} to 2.5 MW.

ELM events on MAST are associated with the radial motion of a poloidally and/or toroidally localised structure away from the outboard separatrix [2]. These events can give rise to strong plasma interaction with surfaces up to 30cm from the plasma edge, but are not associated with any broadening in the divertor target profiles. They are observed on Thomson scattering profiles taken close to the ELM peak, in mid-plane D_α emission and with the mid-plane reciprocating probe, which has been used to determine the radial expansion velocity, v_R. The average $v_R \sim 1.2$ km/s but appears to vary from 200 m/s to 2 km/s for otherwise similar ELMs. The particle flux arriving at the reciprocating probe during these events can be of the same magnitude as that at the divertor targets ($j_{sat} \sim$ 10-100 kAm^{-2}) but can also vary, by up to an order of magnitude, for otherwise similar ELMs.

4. Asymmetric divertor biasing

Toroidally continuous, asymmetric biasing of divertor components is being explored on MAST as a means of broadening Δ_h^t, to reduce the target power loads. This technique may have applications to next-step fusion devices, overcoming the link between D_h and core plasma parameters, such as P_{SOL} (see section 2.2). This is the first time such a scheme has been employed on any tokamak Six of the twelve lower divertor ribs are isolated from the MAST vessel and have been positively biased with up to 120 V at 3kA. The biased ribs alternate with the remaining six unbiased, grounded ribs. The preliminary results indicate that convective cells driven by an **E**x**B** drift are formed in the SOL as a consequence of biasing and that their impact is limited to the divertor leg below the X-point, as predicted by theory [14]. These convective cells have a significant impact on both Δ_h^t and the position of peak heat flux, figure 7. Biasing in L-mode plasmas shows several characteristics in qualitative agreement with theory and demonstrates clear evidence for both SOL broadening and divertor power reduction. Biasing has also been applied to ELMy H-mode plasmas without any indications of, for example, an unwanted transition to L-mode. Several aspects of these observations, however, are yet to be fully understood and, in particular, differences between the grounded and biased ribs during biasing. Future analysis of temperature profiles along the ribs, obtained during these experiments using a fast IR camera, will allow derivation of the heat flux profiles which should help resolve these issues.

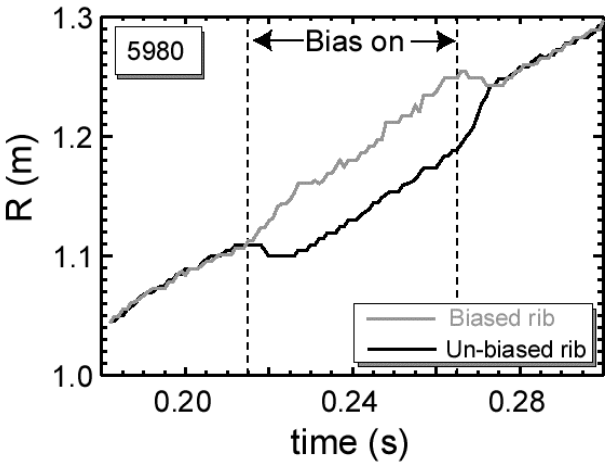

Figure 7: Movement of target peak heat flux (estimated from D_a peak) relative to natural sweeping of strike points during biasing

5. VDEs and halo currents

The isolation of divertor ribs on MAST, necessary for biased divertor studies, has also allowed measurement of halo currents using series resistors, to complement those from an extensive set of magnetic halo current diagnostics. For pre-disruption plasma currents, I_p>300kA, the halo current fraction ($d=I_H/I_p$) is always less than 30% and the maximum observed I_H, for I_p up to 1.2MA, is ~200kA. Toroidal peaking factors up to 1.9 are observed at low d and increase with

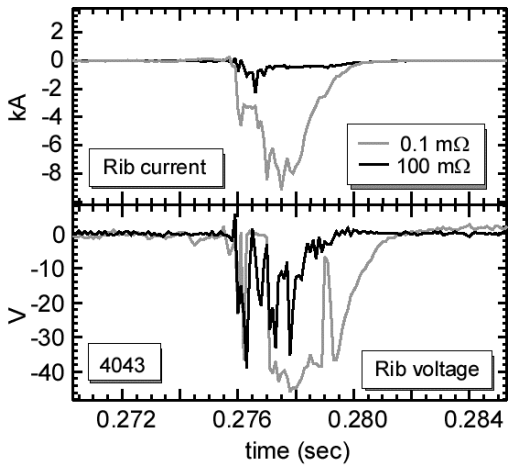

Figure 8:Induced voltages and currents to divertor ribs during VDE

edge safety factor (measured just before the VDE). However, the maximum product of the toroidal peaking factor and *d* remains below 0.3, around half the ITER design limit. Recent studies varying the series resistance on one of the ribs have demonstrated that, whilst the induced voltage remains roughly constant at 30 – 40 V as the resistance is increased (from 0.1 mΩ to 100 mΩ and even 3 kΩ, in some experiments), I_H falls from a typical value of 10 kA to a few hundred Amps or less, figure 8. The halo current flowing in the remaining ribs is unchanged within errors. The plasma therefore seems to behave more as a voltage than a current source, indicating that it may be possible to alter the preferred halo current path and limit the halo current in sensitive components in a next-step device, such as ITER, by adjusting the resistance in a particular path.

6. Conclusions

Divertor power handling in the ST is of even greater significance than in conventional devices due to the reduced major radius, and thus wetted area, of the strike points. The boundary plasma and divertor of a large ST, MAST, have now been characterised in detail for the first time. Results of these studies are contributing not only to research on the ST but also to understanding of the boundary plasma in conventional tokamaks and to preparations for ITER. For example, SOL heat flux width scalings confirm several dependencies exhibited in scalings from multi-machine databases, including a weak negative dependence on power flow across the separatrix. Observations have been made of significant radial efflux into the far SOL during ELMs, which if exhibited on ITER could give rise to substantial first wall erosion. First attempts to actively broaden the target heat flux width by toroidally continuous, asymmetric biasing of the divertor have been tried with some success. Schemes to modify this technique for use on a next-step device are under consideration. Analysis of halo currents during VDEs has indicated a mechanism by which a preferred halo current path can be imposed on the plasma during VDEs.

This work has been jointly funded by Euratom and UK Department of Trade and Industry.

References

[1] B. Lloyd *et al*, this conference
[2] G.F. Counsell *et al*, Plasma Phys. And Control. Fusion 44 (2002) 827
[3] A. Tabasso *et al*, Proc. 15th PSI, Gifu to be published in Journal of Nuclear Materials
[4] A. Loarte, Journal of Nuclear Materials 290-293 (2001) 805
[5] G.F. Counsell *et al*, Proc. 28 EPS Conf. on Plas. Phys. and Contr. Fus., ECA **25A** (2002)
[6] A. Loarte *et al*, Journal of Nuclear Materials, 266-269 (1999) 91
[7] J.W. Conner *et al*, Nuclear Fusion 39 (1999) 169
[8] P.C Stangeby *et al*, Nuclear Fusion 28 (1988) 1945
[9] A. Kirk *et al*, to be submitted to Plasma Physics and Controlled Fusion (2002)
[10] A.B. Mikhailovskii *et al*, Plasma Phys. Rep. **23** (1997) 844
[11] H.R. Wilson, Physics of Plasmas 9 (2002) 1277
[12] R. Buttery *et al*, this conference
[13] A. Herrmann *et al*, Proc. 29 EPS Conf. on Plas. Phys. and Contr. Fus., ECA **26B** (2002) 1180
[14] R.H. Cohen and D.D. Ryutov, Nucl. Fusion 37 (1997) 621